Journal of Bioenergetics and Biomembranes, Vol. 26, No.1, 1994

Modeling a Conformationally Sensitive Region of the Membrane Sector of the Fungal Plasma Membrane Proton Pump

Brian C. Monk,[1,4] Waldo C. Feng,[2] Craig J. Marshall,[5] Donna Seto-Young,[1] Songqing Na,[3] James E. Haber,[3] and David S. Perlin[1,6]

Received May 8, 1993; accepted June 28, 1993

A molecular model for transmembrane segments 1 and 2 from the fungal proton pumping ATPase has been developed, and this structure is predicted to form a helical hairpin loop structure in the membrane. This region was selected because it is highly conformationally active and is believed to be an important site of action for clinically important therapeutics in related animal cell enzymes. The hairpin loop is predicted to form an asymmetric tightly packed structure that is stabilized by an N-cap between D140 and V142, by hydrogen bonding between residues in the turn region and the helices, and by $\pi-\pi$ interactions between closely apposed aromatic residues. A short four-residue S-shaped turn is stabilized by hydrogen bonding but is predicted to be conformationally heterogeneous. The principal effect of mutations within the hairpin head region is to destabilize the local close packing of side groups which disrupts the pattern of hydrogen bonding in and around the turn region. Depending on the mutation, this causes either a localized or a more global distortion of the primary structure in the hairpin region. These altered structures may explain the effects of mutations in transmembrane segments 1 and 2 on ATP hydrolysis, sensitivity to vanadate, and electrogenic proton transport. The conformational sensitivity of the hairpin structure around the S-turn may also account for the effects of SCH28080 and possibly ouabain in blocking ATPase function in related animal cell enzymes. Finally, the model of transmembrane segments 1 and 2 serves as a template to position transmembrane segments 3 and 8. This model provides a new view of the H^+-ATPase that promotes novel structure/function experimentation and could serve as the basis for a more detailed model of the membrane sector of this enzyme.

KEY WORDS: H^+-ATPase; molecular modeling; helical hairpin; aromatic slipper; coupling; molecular dynamics, yeast.

INTRODUCTION

The fungal plasma membrane H^+-ATPase is an electrogenic proton pump within the extended family of P-type ion translocating ATPases. The enzyme has been extensively studied at the biochemical and genetic level (Serrano, 1988). It is a conformationally active polytopic membrane protein that is tightly regulated and essential for growth (Serrano *et al.*, 1986). A fundamental property of the P-type ATPases is an ability to couple energy from ATP hydrolysis in a cytoplasmically located catalytic domain to ion transport in the membrane-embedded region of the protein. Numerous studies support the notion of coupling or functional interaction between the ion transport and ATP hydrolysis domains (Glynn and Karlish, 1990). The effects of the cardiac glycoside

[1] Department of Biochemistry, The Public Health Research Institute, 455 First Avenue, New York, New York 10016.
[2] Department of Physiology and Biophysics, Mount Sinai School of Medicine, 1 Levy Place, New York, New York 10029.
[3] Rosenstiel Basic Medical Sciences Research Center and the Department of Biology, Brandeis University, Waltham, Massachusetts 02254.
[4] Experimental Oral Biology Unit, Faculty of Dentistry, University of Otago, Dunedin, New Zealand.
[5] Department of Biochemistry, University of Otago, Dunedin, New Zealand.
[6] To whom correspondence should be addressed.

0145-479X/94/0200-0101$07.00/0

ouabain on the Na^+,K^+-ATPase best illustrates such coupled interactions. This potent inhibitor is believed to bind at an exposed extracellular site on the enzyme and exerts, at a considerable distance, a pronounced effect on the ATP hydrolysis reaction within the cytoplasmically located catalytic center (Forbush, 1983, Price *et al.*, 1990). The actual coupling distance is difficult to quantify but the distance between sites within the catalytic center and membrane-embedded ion transport region has been estimated to exceed 40 Å for the related Ca^{2+}-ATPase (Bigelow and Inesi, 1991).

The structural basis for long-range coupling between disparate domains is not understood. However, a growing body of experimental data from genetic (Rabon *et al.*, 1988; Price *et al.*, 1990; Harris *et al.*, 1991; Na *et al.*, 1993), immunochemical (Arystarkhova *et al.*, 1992), and drug interaction (Munson *et al.*, 1991) studies on the H^+-ATPase, Na^+,K^+-ATPase, Ca^{2+}-ATPase, and H^+,K^+-ATPase support a conformational interaction between transmembrane helices 1 and 2 and the catalytic sector. Again, the effects of cardiac glycosides may be the most informative. The affinity of the Na^+,K^+-ATPase for oubain can be substantially altered ($\sim 10^4$ fold) by mutations in the loop region between transmembrane segments 1 and 2 (Price *et al.*, 1989; Price *et al.*, 1990), by mutation of a Cys residue (C113 in the *X. laevis* Na^+, K^+-ATPase) within transmembrane segment 1 (Canessa *et al.*, 1992), or by chemical modification of Cys residues (C637 and C656) in the catalytic center (Kirley and Peng, 1991). In addition, a monoclonal antibody recognizing an epitope in the external loop region between transmembrane segments 1 and 2 in the Na^+,K^+-ATPase potentiates the inhibitory effects of ouabain and also inhibits enzyme activity by itself (Arystarkhova *et al.*, 1992). Similar interactions between functional domains have been found in the yeast H^+-ATPase by studying the effects of second-site suppressor mutations. A primary site mutation, S368F, near the site of phosphorylation (D378) was found to be partially suppressed by mutations in transmembrane segments 1 and 2 (Harris *et al.*, 1991). More recently, it was found that an A135V mutation close to the cytoplasmic face of transmembrane segment 1 was fully suppressed by several second-site mutations, including one within the putative cytoplasmic ATP hydrolysis domain (Na *et al.*, 1993). Finally, a study on the potent H^+,K^+-ATPase inhibitor SCH28080 suggested a putative binding site for this drug within the loop region between transmembrane segments 1 and 2 (Munson *et al.*, 1991).

A clearer understanding of how a conformationally sensitive region contained within transmembrane segments 1 and 2 can interact with the catalytic domain requires a greater understanding of molecular enzyme structure. Unfortunately, the structure of the ATPase is poorly understood. In general, the structural analysis of membrane proteins poses a set of experimental problems that is especially difficult to circumvent with current techniques. Computer-assisted molecular modeling of the membrane bound regions may provide an alternative approach to the generation of structural information. Molecular modeling is most useful for the visualization and refinement of known protein structures, but it has also been valuable, within limits, as a predictive tool of protein structure (DeGrado *et al.*, 1989; Findlay *et al.*, 1990; Sali *et al.*, 1990; Thornton and Gardner, 1990).

Molecular modeling of membrane-bound regions and its experimental refinement through biochemical and genetic manipulation may provide an alternative approach for structure studies of membrane proteins which cannot be readily studied with X-ray crystallography (Findlay *et al.*, 1990). Information obtained from the comparative analysis of primary sequences, when combined with structural, functional, and biogenic constraints intrinsic to imbedding integral membrane proteins into the lipid bilayer, can provide a basis for the construction of simple molecular models. Sachs and colleagues recently proposed a model for transmembrane segments 1 and 2 in the gastric H^+,K^+-ATPase based on topological considerations, and its interaction with the inhibitor SCH28080 (Munson *et al.*, 1991). In principle, such models can be tested, extended, and refined with supporting data from genetic and spectroscopic analyses.

In this report, a detailed molecular model for transmembrane segments 1 and 2 of the yeast H^+-ATPase has been developed by combining molecular structure modeling with analyses of mutational data, conserved residues, and conserved protein stabilizing features. The model serves as a template to dock interacting transmembrane segments 3 and 8, and could provide the basis for a more inclusive model encompassing the entire membrane sector of the enzyme.

MATERIALS AND METHODS

Model Building

Transmembrane helices 1 and 2 of the *S. cerevisiae* H^+-ATPase were constructed with the molecular modeling program QUANTA (Polygen, Inc., v. 3.00) on a Silicon Graphics IRIS computer (Model 4D/70GT). Alpha helices were assigned to residues F116-G137 and V142-F163 corresponding to transmembrane segments 1 and 2, respectively. Residues G137-W141 comprise the tight S-turn between transmembrane segments 1 and 2. Mutations were introduced through molecular replacement of the initial wild-type cartesian coordinate system. All equivalent atoms between the original and the mutated transmembrane helices were conserved while dissimilar atoms were constructed from a standard residue topology file. Thus, the protein backbone remained unaltered for all the mutants. The modeled mutations include A135V, A135F, and A135V/V135F.

All four structures (WT, A135V, A135F, and A135V/V157F) were energetically minimized with the steepest descent algorithm for 15,000 steps or until convergence of 0.01 kcal/mol was established. A short molecular dynamics (Discover, Biosym Tech., v. 2.7.0) simulation (60 psec) at room temperature (300°K) was performed for each structure. Three structural components of the transmembrane model were energetically constrained during the simulation. A harmonic force constant was used to tether the sidechains of the three phenylalanines (F119, F159, F163) which comprise the aromatic slipper, the N cap atoms (amide H of D140 and the carboxyl O of V142), and a positional constraint was used to fix the N and C terminal residues. A molecular dynamics (MD) averaged conformer (50 psec) was determined from the equilibrated period of the simulation. Each MD-averaged structure was then energy minimized with steepest descent for 15,000 steps or until a convergence of 0.01 kcal/mol was established. All comparisons and analyses of the transmembrane helices were made from these minimized MD-averaged structures.

RESULTS AND DISCUSSION

Modeling Transmembrane Segments 1 and 2 as a Helical Hairpin

A considerable amount of evidence from chemical and immunochemical studies of the H^+-ATPase (Mandala and Slayman, 1989; Hennesey and Scarborough, 1990; Monk *et al.*, 1991; Rao *et al.*, 1991; Seto-Young *et al.*, 1992), as well as of other P-type enzymes (Munson *et al.*, 1991; Feschenko *et al.*, 1992; Mata *et al.*, 1992; Modyanov *et al.*, 1992; Sachs *et al.*, 1992), supports a topological organization for transmembrane segments 1 and 2 in which the N- and C-terminal extensions from these segments are cytoplasmically exposed whereas the linking region is extracytoplasmically exposed. This region of the H^+-ATPase (F116-F163 of the *S. cerevisiae* H^+-ATPase) has been modeled as a helical hairpin loop structure that is dominated by a pair of membrane-spanning antiparallel α-helices (F116-G137; W141-F163) (Fig. 1A). A four-residue S-shaped turn joins the two helices and is sufficient to reverse the orientation of the helices without introducing packing difficulties (Fig. 1B). The central portion of the turn is made up of the polar S139 and the charged D140 residue. Residues L138 and D140 contribute the edges of the turn structure, with each residue retaining a single hydrogen bond to its parent helix. The conformation of the turn is stabilized by two hydrogen bonds involving a conserved pair of acidic residues, D140 and D143 (Fig. 2). The carboxyl of the D140 side chain forms a hydrogen bond, with the amide nitrogen of V142 forming an N-cap (Richardson and Richardson, 1988). The carboxylic side chain of D143 forms a hydrogen bond with the backbone amide between S139 and D140. The hydrogen bonds between D140 and D143 are considered important structural constraints in the model. Both residues are absolutely conserved in the fungal proton pumping ATPases, suggesting that they may be important structural and/or functional elements. Modification of D143 to Glu or Ala produces a dominant lethal mutation (Seto-Young, Monk, Na, Haber, and Perlin, unpublished), whereas a D143N modification produces a wild-type phenotype (Serrano and Portillo, 1990) possibly because it can maintain the hydrogen bonding potential of the side chain. Unlike D140 or D143, the residue equivalent to S139 varies considerably in fungal H^+-ATPases (Fig. 3). It is observed as Glu in *C. albicans* and *N. crassa*, and as Arg in *S. pombe*. The conformational sensitivity of the turn between transmembrane segments 1 and 2 is affirmed by the loop mutations L138Y and D140E which confer growth resistance to hygromycin B (Monk and Perlin, unpublished). This phenotype has been correlated with a depolarized cellular

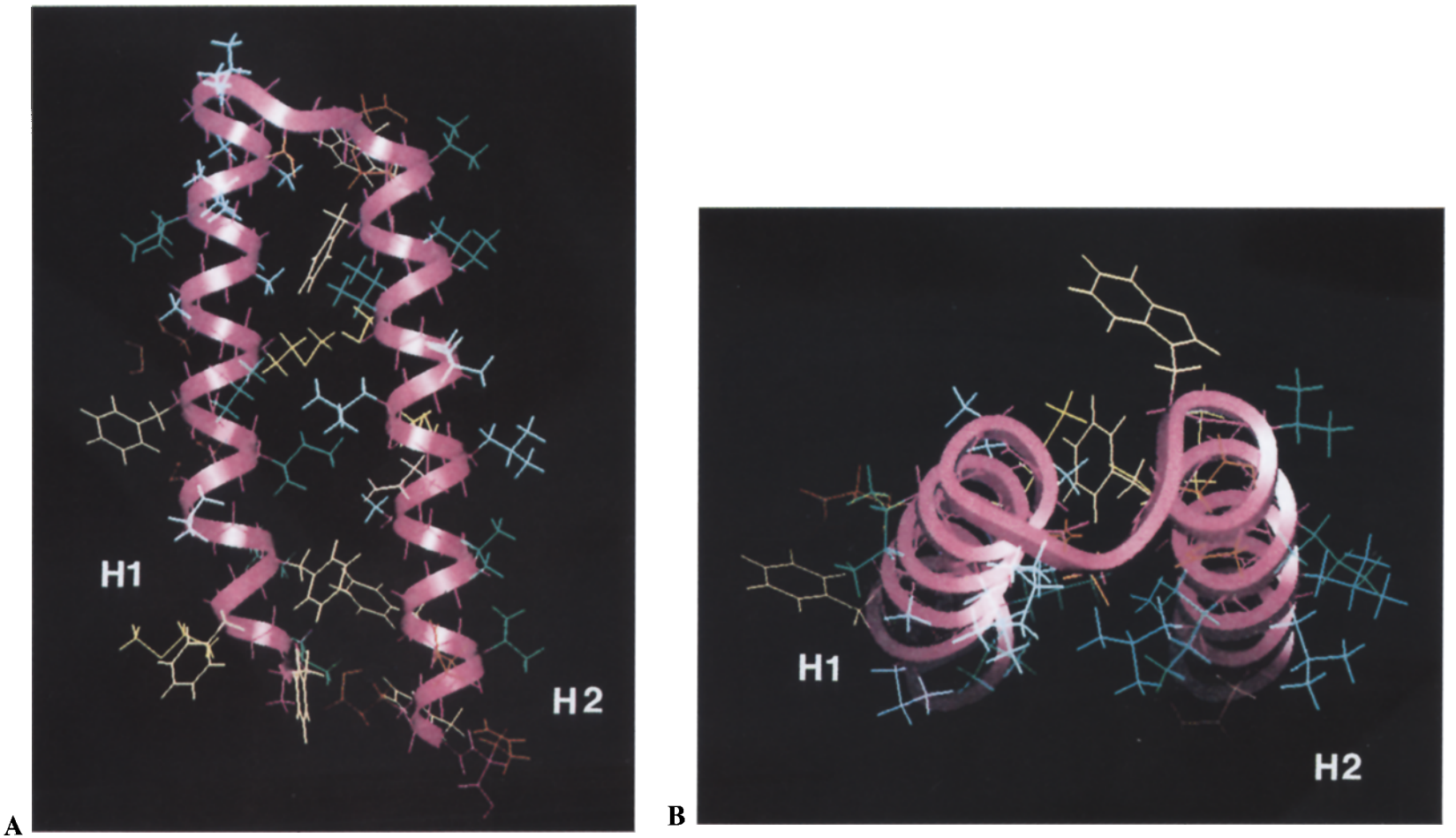

Fig. 1. Helical hairpin loop model of transmembrane segments 1 and 2. A solid ribbon diagram superimposed on the carbon backbone of amino acid residues F116–F163 of the *S. cerevisiae* H^+-ATPase which comprise transmembrane segments 1 and 2. (A) Model view parallel to the plane of the bilayer. (B) Model view from the extracytoplasmic surface nearly perpendicular to the plane of the bilayer.

membrane potential due to a defect in electrogenic proton transport by the H^+-ATPase (Perlin *et al.*, 1988). In addition, modification of the turn region by insertion of additional residues between L138 and S139 perturbs enzyme activity in a steric- and charge-dependent manner (Seto-Young, Monk, Na, Haber and Perlin, manuscript in preparation).

The simple S-shaped linkage between the two antiparallel α-helices helps maintain the hairpin structure in a tightly packed configuration. The interdigitation of amino acid side chains between the adjacent helices encourages a small angular displacement between the helices analogous to that found between helices 1 and 2 of a four helix bundle (Chou *et al.*, 1988). A reflection of the close contact between the helix pair near the turn is the enrichment for alanine residues on the face of transmembrane segment 1 immediately underlying the turn region. Bulkier side chains near the cytoplasmic ends of the hairpin loop fill the additional space between the two helices. These side chains lie below a conserved proline residue (P123.) A proline-induced kink in the helix of approximately 26° is expected to align the cytoplasmic ends of the helices more parallel to each other (Fig. 1B). Such motifs are frequently observed within the transmembrane portions of membrane proteins (Brandl and Deber, 1986). It is noteworthy that the predicted helical hairpin structure of transmembrane segments 1 and 2, which contains a proline kink within close proximity to a buried acidic residue (E129) in transmembrane helix 1, is strikingly similar to the structure predicted for the proteolipid of proton-translocating F_0F_1-type ATPases (Miller *et al.*, 1990).

Tight Packing of Transmembrane Segments 1 and 2 and its Consequences

The insertion of bulky residues close to the turn should cause the greatest relative displacement of the hairpin loop; whereas bulky residues inserted nearer the cytoplasmic face of the membrane should cause the least conformational change. The function-altering A135V and A135F mutations in the *S. cerevisiae* enzyme lie at the transition between the C-terminus of helix 1 and the S-turn, and confer hygromycin B resistance and low pH sensitivity on whole cells; the mutant ATPases show less than 30% of wild-type activity (Table I), which appears to result from a structural instability (Na *et al.*, 1993). The effects of the mutations on the hairpin model were initially evaluated by introducing the mutant residues into the wild-type structure and energy minimizing the resulting structure. This static view produced a minor average displacement (RMS < 1 Å) of the hairpin backbone with most of the effects being observed in the turn region. Due to the tightly packed nature of this region, it was apparent that a more valuable representation of the mutational effects would come from allowing the structure to explore its full conformational space in molecular dynamic simulations. This powerful approach examines the fluctuations of the relative positions of atoms in a protein as a function of time, which in turn can provide a measure of the internal motion of a protein (Karplus and Petsko, 1990). Wild-type and mutant energy-minimized structures were subjected to molecular dynamic simulation. The minimized average structures from the simulations were compared, and the positional displacements (RMS) from the wild-type structure were plotted as a function of amino acid (Fig. 4). The most significant differences (RMS > 2 Å) were observed from residues A135–I146 for the A135V mutation, whereas the bulkier A135F mutation distorted the backbone structure of both helices to much greater extent (Fig. 4A). These global distortions are consistent with the diminished activity of the A135F enzyme relative to the A135V enzyme and the tight packing of the hairpin region in the wild-type enzyme (Na *et al.*, 1993). An equally significant finding is that the hydrogen-bonding profiles of the mutant structures, A135V and A135F, are significantly altered relative to wild type in and around the turn region (Table II). This is important because H-bonding is expected to play a major stabilizing role in the model structure. Finally, a suppressor mutation V157F that largely restores the activity of the A135V mutation (Na *et al.*, 1993) had little effect on the displacement of helix 1 but did reduce the large displacement observed at the N-terminus of helix two (Fig. 4B). As expected, the H-bonding profile for the double mutant in helix 2 was closer to that of wild type than the A135V mutant alone. This result suggests that alterations in catalysis may be more closely tied to perturbations in helix 2. All the analyzed structures (wt, A135V, A135F, A135V/V157F) appeared conformationally heterologous in the turn region, suggesting that it is the least constrained and most conformationally flexible portion of the hairpin. This suggestion is also consistent with the fact that the turn region shows significant variation among the P-type ATPases, ranging from four residues in

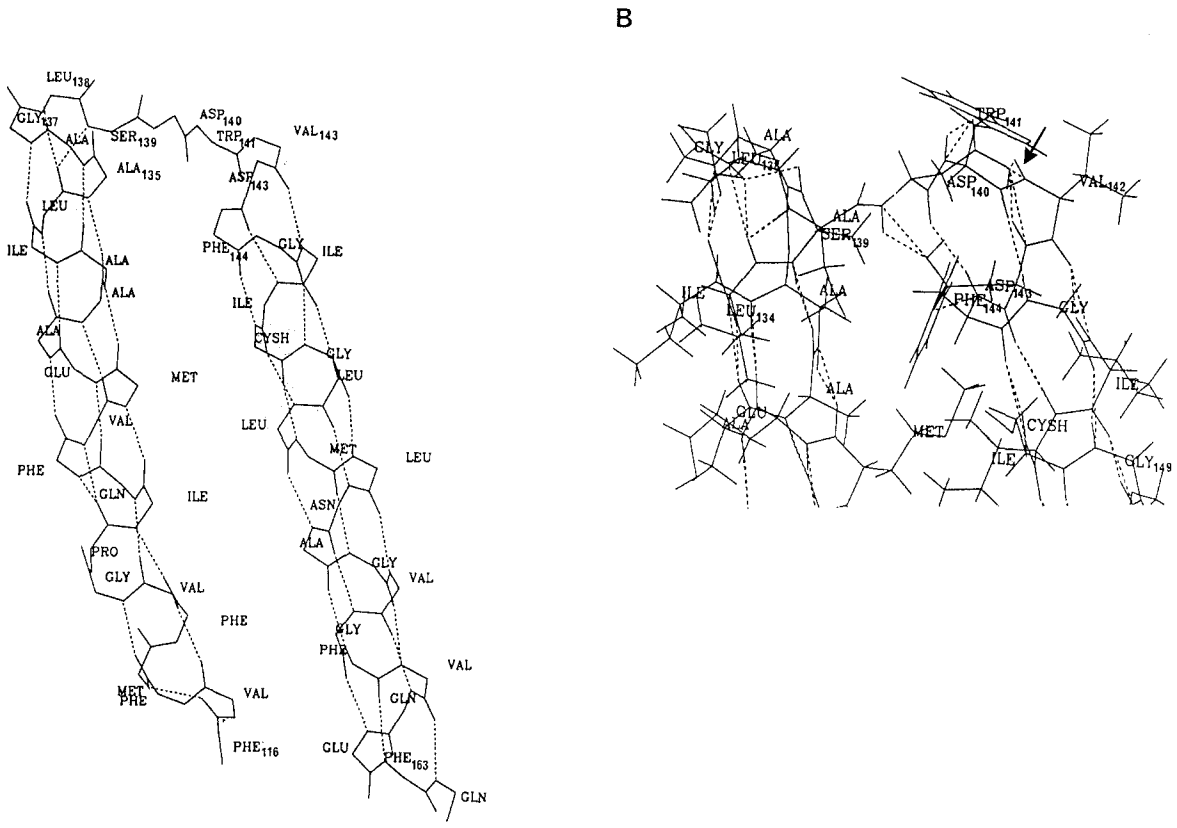

Fig. 2. Hydrogen bonding profile for the helical hairpin structure. (A) Hydrogen bonding shown for the helical segments encompassing amino acids F116–G137 and V142–F163. (B) Detail of amino acid residues E129–G149 which highlights the turn region between transmembrane segments 1 and 2 and stabilizing hydrogen bonding. The N-cap structure and the atoms involved in hydrogen bonding between D140 and V142 are shown by the arrow.

GENE	HELIX 1	TURN	HELIX 2
ScPMA1	F_{116}VMFFVGPIQFVMEAAAILAAG	LSDW	VDFGVICGLLMLNAGVGFVQEF
ScPMA2	F_{145}LMFFVGPIQFVMEAAAILAAG	LSDW	VDVGVICALLLLNASVGFIQEF
CaPMA1	F_{93} VMFFVGPIQFVMEAAAVLAAG	LEDW	VDFGVICALLLLNAFVGFIQEY
SpPMA1	F_{114}IMFFVGPIQFVMEMAAALAAG	LRDW	VDFGVICALLMLNAVVGFVQEY
SpPMA2	F_{202}LSFFVGPIQFVMELAAALAAG	LRDW	VDFGVICALLLLNATVGFVQEY
NcPMA1	F_{116}LGFFVGPIQFVMEGAAVLAAG	LEDW	VDFGVICGLLLLNAVVGFVQEF
ZrPMA1	F_{118}LMFFIGPIQFVMEAAAVLAAG	LEDW	VDFGYICGLLFLNAGVGFIQEF
LdPMA1	Y_{91} VRGLWGPMPAALWIAIIIEFA	LENW	PDGAILFAIQIANATIGWYETI
AtAHA1	F_{61} LGFMWNPLSWVMEAAALMAIA	LANGDNRPPDW	QDFVGIICLLVINSTISFIEEN
LeLHA1	F_{65} LGFMWNPLSWVMEAAAIMAIA	LANGGGKPPDW	QDFVGIITLLIINSTISFIEEN
HK	L_{105}AGGLQCLMWVAAAICLIAFAI	QASEGDLTTDDN	LYLALALIAVVVVTGCF
NaK	Q_{93}LFGGFSMLLWIGAVLCFLAYGIQAA	TEEEEPQN	DNLYLGVVLSAVVIITGCFSYYQ
Ca-PM	E_{104}ALQDVTLILILEIAAIVSLGLSFYQ	PPEGDNALCGEVSVGEEEGEGET	GWIEGAAILLSVVCVVLVTAFNDWS
Ca-Sr	L_{60}LVRILLLAACISFVLAWF	EEGEETIT	AFVEPFVILLILVANAIVGVW

Fig. 3. Comparison of P-type ATPase sequences corresponding to transmembrane segments 1 and 2. The deduced amino acid sequences from *PMA1* and *PMA1*-like genes encoding H^+-ATPases from *Saccharomyces cerevisiae* (Sc), *Candida albicans* (Ca), *Schizosaccharomyces pombe* (Sp), and *Neurospora crassa* (Nc), *Zygosaccharomyces rouxii* (Zr), *Leishmania donovani* (Ld), *Arabidopsis thaliana* (At), *Lycopersicum esculentum* (Le), and the α-subunit genes from the H^+,K^+-ATPase (HK; rat stomach), Na^+,K^+-ATPase (NaK; sheep muscle), Ca^2-ATPase (Ca-PM; rat brain plasma membrane) and Ca^{2+}-ATPase (Ca-Sr; rabbit muscle sarcoplasmic reticulum) were compared. The *PMA*1, *PMA2*, *AHAL*, *LHAL*, Ca^{2+}-ATPase (Ca-PM), and Na^+,K^+-ATPase sequence alignments were adapted from Wach *et al.* (1992). The H^+,K^+-ATPase sequence was from Shull and Lingrel (1986), and the Ca^{2+}-ATPase (Ca-Sr) sequence was from MacLennan *et al.* (1985).

Table I. Properties of *pma1* Mutants[a] Mapping to Hairpin Region

	Cellular phenotype		Biochemical properties	
Mutation	Hygromycin B^r	Low pH^s	ATPase[b] (% of control)	Proton transport[c] (% quench/min)
Wild Type	No	No	100	55.4
A135V	Yes	Yes	33	1.8
A135F	Yes	Yes	15	1.8
A135G	Yes	No	71	53.6
A135V, V157F	No	No	39	54.7
A135L	Yes	Yes	50	15.4
A135R	Recessive lethal[d]			
A135E	Recessive lethal			
A135S	Dominant negative[e]			
A135W	Dominant negative			

[a]All mutants were described by Na *et al.* (1993).
[b]ATPase specific activities were determined for plasma membrane-bound enzymes.
[c]Proton transport was assessed for purified enzyme reconstituted into liposomes.
[d]Recessive lethal phenotypes reflect mutations which can be maintained stably with a wild-type *PMA1* gene in a diploid cell. Upon sporulation, the cell yields two wild-type spores and two dead mutant spores.
[e]Dominant negative phenotypes arise when a mutation cannot be maintained stably with the wild-type *PMA1* gene in a diploid cell and there is selection pressure for gene replacement. The diploid cell in this case produces all wild-type spores upon sporulation.

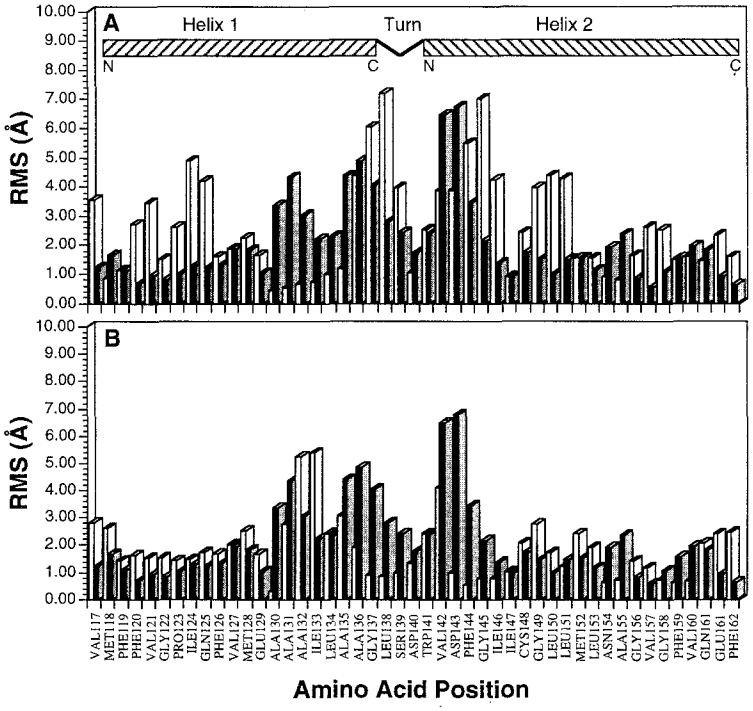

Fig. 4. Positional displacement of individual main chain atoms for *pma1* mutant structures relative to wild type following molecular dynamics simulation. A molecular dynamics-averaged (50 psec) structure was determined for defective *pma1* mutants A135V and A135F, and suppressor double mutant A135V/V157F. The coordinate difference of main chain atoms (Å) for the mutant structures relative to a standard wild-type structure was plotted as a function of the wild-type amino acid sequence for A135V (closed bars) and A135F (open bars) in Panel A, and A135V (closed bars) and A135V/V157F (open bars) in Panel B.

the fungal H^+-ATPases to 23 residues in the Ca^{2+}-ATPase (Fig. 3).

Disruption of packing in the region localized around A135 is clearly deleterious to ATPase activity and cell growth, and the strength of these effects correlates well with the steric size (V < L < F) of the mutant side chain (Na *et al.*, 1993). Interestingly, the A135I mutant does not precisely conform to this pattern, behaving with properties intermediate between the A135V and A135L mutants. This behaviour suggests that the stereochemistry of the beta-carbon substituents of the mutant side chain may also affect packing. Replacement of A135 with either a positively charged arginine, a negatively charged glutamic acid, or a polar serine residue leads to cell death. These results indicate that the environment in this region is hydrophobic and that the insertion of bulky charged groups or a relatively small polar group is even more destabilizing than the addition of bulky hydrophobic groups. Replacement of A135 with glycine, which may introduce a small destabilizing hydrophobic cavity, also alters ATPase function (Na *et al.*, 1993). Such cavities in the interior of T4 lysozyme give conformations that are less stable than the wild-type enzyme (Eriksson *et al.*, 1992). The collection of altered physiological and biochemical phenotypes conferred by mutations in the modeled region of the ATPase is consistent with the notion that structural perturbations underlying the turn between transmembrane segments 1 and 2 can be transmitted across the lipid bilayer to catalytic elements of the ATPase molecule.

The Aromatic Slipper

Many of the aromatic side chains located toward the cytoplasmic end of transmembrane segments 1 and 2 appear to be nested and overlapping (Fig. 5). These nested aromatics form a type of "aromatic slipper" because of the way the side chains interdigitate. The aromatic amino acids in this region are identical among the fungal ATPases, apart from a single conservative Phe (F163) to Tyr change in *C. albicans*, suggesting that they may be important determinants in structure. The aromatic residues interfacing between transmembrane segments 1 and 2 are proposed to lie at right angles to one another in a T-type structure, as has been observed in crystalline benzene (Hunter and Sanders, 1990). The positive interaction of such groups mediated by π-interactions between the negatively charged field of the *p*-orbitals perpendicular to the plane of the aromatic rings and the partial positive charges of atoms in the ring is expected to be strongly stabilizing. The electrostatic component of this type of interaction, although smaller than the Van der Waals contribution, is likely to dominate the geometry between helical segments within a hydrophobic environment (Hunter *et al.*, 1991). Cores of aromatic residues are important in the folding of many proteins. This is likely because aromatic residues are both hydrophobic and lipophobic. They are therefore expected to seek complementary surfaces (i.e., other aromatic sidechains) rather than ordering the surrounding aqueous phase or distorting the core of the lipid bilayer. For example, a soluble thermolytic fragment of colicin A has a cluster of Trp and Tyr residues that is believed to stabilize a hydrophobic hairpin at the center of its 10-helix structure (Suga *et al.*, 1991). Furthermore, the c-myb protooncogene product has a set of three conserved Trp residues in the DNA binding domain that is predicted to form aromatic clusters contributing to both protein folding and regulatory function (Kanei-Ishii *et al.*, 1990). In the fungal ATPases, aromatics could play a role in loop formation by stabilizing the initial folding of the two transmembrane helices prior to or during membrane insertion.

An interesting consequence of the nested aromatics is that aromatic *p*-orbitals could be polarized by the application of a voltage across the membrane. Depending on the field direction, the π-electrons would become unequally distributed, giving a net negative charge at one or the other end of the aromatic ring relative to the γ-carbon. This polarizing effect could alter the geometry of interaction between nested aromatics, with interacting aromatic rings partitioning between T-structures and offset-antiparallel structures, as has been observed in model studies (Hunter and Sanders, 1990; Hunter *et al.*, 1991). It is well known that the H^+-ATPase is sensitive to applied voltage (Seto-Young and Perlin, 1991), and the imposition of an electric field could directionally modify a conformationally sensitive region that is believed to interact with the catalytic ATP hydrolysis domain.

Expanding the Two-Helix Model to include Transmembrane Segments 3 and 8.

A single disulfide linkage in the *N. crassa* plasma membrane ATPase has been identified between C148 and either C840 or C869 (Rao and Scarborough, 1990). Based on the conservation of cysteine residues among fungal plasma membrane H^+-ATPases, we

Table II. Detailed Hydrogen-Bond Profile for Wild-Tyle and *pma1* Mutant Structures[a]

	Donor		Acceptor		
Residue	Atom 1	Atom 2	Atom 3	Atom 4	Residue
PMA1 (wt)					
MET118	118 N	118 H	115 O	115 C	PHE115
PHE119	119 N	119 H	115 O	115 C	PHE115
GLY122	122 N	122 H	118 O	118 C	MET118
ILE124	124 N	124 H	120 O	120 C	PHE120
GLN125	125 N	125 H	121 O	121 C	VAL121
GLN125	125 NE2	125 HE21	125 O	125 C	GLN125
PHE126	126 N	126 H	122 O	122 C	GLY122
VAL127	127 N	127 H	123 O	123 C	PRO123
ALA130	130 N	130 H	126 O	126 C	PHE126
ALA131	131 N	131 H	127 O	127 C	VAL127
ALA132	132 N	132 H	128 O	128 C	MET128
ILE133	133 N	133 H	129 O	129 C	GLU129
LEU134	134 N	124 H	130 O	130 C	ALA130
ALA 135	135 N	135 H	131 O	131 C	ALA131
GLY137	137 N	137 H	139 O	139 C	SER139
LEU138	138 N	138 H	134 O	134 C	LEU134
SER139	139 N	139 H	134 O	134 C	LEU134
ASP140	140 N	140 H	139 OG	139 CB	SER139
ASP140	140 N	140 H	143 OD2	143 CG	ASP143
TRP141	141 N	141 H	135 O	135 C	ALA135
VAL142	142 N	142 H	140 OD1	140 CG	ASP140
ASP143	143 N	143 HD2	143 O	143 C	ASP143
GLY145	145 N	145 H	142 O	142 C	VAL142
CYS148	148 N	148 H	144 O	144 C	PHE144
GLY149	149 N	149 H	145 O	145 C	GLY145
LEU150	150 N	150 H	146 O	146 C	ILE146
LEU151	151 N	151 H	147 O	147 C	ILE147
MET152	152 N	152 H	148 O	148 C	CYS148
ASN154	154 N	154 H	150 O	150 C	LEU150
ALA155	155 N	155 H	151 O	151 C	LEU151
GLY156	156 N	156 H	151 O	151 C	LEU151
GLY158	158 N	158 H	154 O	154 C	ASN154
PHE159	159 N	159 H	155 O	155 C	ALA155
VAL160	160 N	160 H	157 O	157 C	VAL157
GLU162	162 N	162 H	158 O	158 C	GLY158
PHE163	163 N	163 H	159 O	159 C	PHE159
GLN165	165 N	165 H	160 O	160 C	VAL160
pma1F135					
VAL117	117 N	117 H	162 OE116	162 CD	GLU161
PHE119	119 N	119 H	116 O	116 C	PHE116
PHE120	120 N	120 H	116 O	116 C	PHE116
VAL121	121 N	121 H	117 O	117 C	VAL117
GLY122	122 N	122 H	117 O	117 C	VAL117
GLN 125	125 N	125 H	121 O	121 C	VAL121
PHE126	126 N	126 H	122 O	122 C	GLY122
VAL127	127 N	127 H	123 O	123 C	PRO123
MET128	128 N	128 H	124 O	124 C	ILE124
GLU129	129 N	129 H	125 O	125 C	GLN125
ALA130	130 N	130 H	126 O	126 C	PHE128
ALA 131	131 N	131 H	127 O	127 C	VAL127
PHE135	135 N	135 H	131 O	131 C	ALA131
ALA136	136 N	136 H	131 O	131 C	ALA131
LEU138	138 N	138 H	134 O	134 C	LEU138

Table II. Continued.

	Donor		Acceptor		
Residue	Atom 1	Atom 2	Atom 3	Atom 4	Residue
SER139	139 N	139 H	134 O	134 C	LEU138
SER139	139 OG	139 HG	139 O	139 C	SER139
ASP140	140 OD2	149 HD2	143 OD2	143 CG	ASP143
TRP141	141 N	141 H	135 O	135 C	PHE135
ASP143	143 N	143 H	140 O	140 C	ASP140
ILE146	146 N	146 H	141 O	141 C	TRP141
CYS148	148 N	148 H	145 O	145 C	GLY145
LEU150	150 N	150 H	146 O	146 C	VAL146
LEU151	151 N	151 H	147 O	147 C	ILE147
ASN154	154 N	154 H	151 O	151 C	LEU151
GLY156	156 N	156 H	152 O	152 C	MET152
VAL157	157 N	157 H	153 O	153 C	LEU153
PHE159	159 N	159 H	155 O	155 C	ALA155
VAL160	160 N	160 H	156 O	156 C	GLY156
GLN161	161 N	161 H	157 O	157 C	VAL157
PHE163	163 N	163 H	159 O	159 C	PHE159
pma1-V135					
MET118	118 N	118 H	115 O	115 C	PHE115
PHE120	120 N	120 H	162 OE1	162 CD	GLU162
GLN125	125 N	125 H	121 O	121 C	VAL121
PHE126	126 N	126 H	122 O	122 C	GLY122
MET128	128 N	128 H	123 O	123 C	PRO123
GLU129	129 N	129 H	124 O	124 C	ILE124
ALA130	130 N	130 H	125 O	125 C	GLN125
ALA131	131 N	131 H	126 O	126 C	PHE126
LEU134	134 N	134 H	131 O	131 C	ALA131
VAL135	135 N	135 H	131 O	131 C	ALA131
ALA136	136 N	136 H	132 O	132 C	ALA132
LEU138	138 N	138 H	133 O	133 C	ILE 133
SER139	139 N	139 H	134 O	134 C	LEU134
SER139	139 OG	139 HG	139 O	139 C	SER139
ASP140	140 N	140 H	138 O	138 C	LEU138
ASP140	140 OD2	140 HD2	137 O	137 C	GLY137
TRP141	141 N	141 H	135 O	135 C	VAL135
VAL142	142 N	142 H	140 OD1	140 CG	ASP140
ILE146	146 N	146 H	144 O	144 C	PHE144
GLY149	149 N	149 H	145 O	145 C	GLY145
LEU151	151 N	151 H	147 O	147 C	ILE147
MET152	152 N	152 H	148 O	148 C	CYS148
ASN154	154 N	154 H	150 O	150 C	LEU150
ALA155	155 N	155 H	151 O	151 C	LEU151
GLY156	156 N	156 H	152 O	152 C	MET152
VAL157	157 N	157 H	153 O	153 C	LEU153
GLY158	158 N	158 H	153 O	153 C	LEU153
PHE159	159 N	159 H	154 O	154 C	ASN154
VAL160	160 N	160 H	156 O	156 C	GLY156
GLN161	161 N	161 H	157 O	157 C	VAL157
GLU162	162 N	162 H	158 O	158 C	GLY158
pma1-V135,F157					
VAL117	117 N	117 H	162 OE1	162 CD	GLU162
PHE119	119 N	119 H	116 O	116 C	PHE116
PHE120	120 N	120 H	116 O	116 C	PHE116
ILE124	124 N	124 H	120 O	120 C	PHE120

Table II. Continued.

Donor			Acceptor		
Residue	Atom 1	Atom 2	Atom 3	Atom 4	Residue
GLN125	125 N	125 H	121 O	121 C	VAL121
PHE126	126 N	126 H	122 O	122 C	GLY122
VAL127	127 N	127 H	123 O	123 C	PRO123
MET128	128 N	128 H	123 O	123 C	PRO123
GLU129	129 N	129 H	124 O	124 C	ILE124
ALA132	132 N	132 H	127 O	127 C	VAL127
ALA136	136 N	136 H	131 O	131 C	ALA131
LEU138	138 N	138 H	133 O	133 C	ILE133
SER139	139 N	139 H	134 O	134 C	LEU134
SER139	139 OG	139 HG	139 O	139 C	VAL135
SER139	139 OG	139 HG	139 O	139 C	SER139
ASP140	140 N	140 H	138 O	138 C	LEU138
ASP140	140 OD2	140 HD2	140 O	140 C	ASP140
TRP141	141 N	141 H	137 O	137 C	GLY137
ASP143	143 OD2	143 HD2	143 O	143 C	ASP143
ILE147	147 N	147 H	143 O	143 C	ASP143
CYS148	148 N	148 H	144 O	144 C	PHE144
LEU150	150 N	150 H	145 O	145 C	GLY145
MET152	152 N	152 H	148 O	148 C	CYS148
LEU153	153 N	153 H	149 O	149 C	GLY149
ASN154	154 N	154 H	150 O	150 C	LEU150
ASN154	154 ND2	154 HD21	150 O	150 C	LEU150
ASN155	155 N	155 H	151 O	151 C	LEU151
GLY156	156 N	156 H	152 O	152 C	MET152
PHE157	157 N	157 H	153 O	153 C	LEU153
GLY158	158 N	158 H	153 O	153 C	LEU153
PHE159	159 N	159 H	155 O	155 C	ALA155
GLN161	161 N	161 H	157 O	157 C	PHE157
GLN161	161 NE2	161 HE21	157 O	157 C	PHE157
GLU162	162 N	162 H	158 O	158 C	GLY158
PHE163	163 N	163 H	159 O	159 C	PHE159

[a] Hydrogen bond profile generated for energy-minimized structures following molecular dynamics simulations.

previously suggested that transmembrane segments 2 and 8 may be linked by a disulfide bridge between C148 and C867 (*S. cerevisiae*) (Harris *et al.*, 1991), although this postulated disulfide is not considered to be essential (Harris *et al.*, 1991). This covalent linkage would restrict the possible conformations of transmembrane segments 1, 2, and 8. Transmembrane segment 8 can be docked into the groove that lies behind the interface formed between transmembrane segments 1 and 2 (Fig. 6). In this position, the aromatic sidechain of F882 is expected to project below the "aromatic slipper" formed between helices 1 and 2. In addition, transmembrane segment 7 is expected to lie beside transmembrane segment 8. The model for transmembrane segments 1, 2, and 8 can be expanded to include transmembrane segment 3 by considering electrostatic interactions between the helices. This speculative alignment of transmembrane segments 1 and 2 with transmembrane segment 3 is in part based on charge complementarity between the asymmetric distribution of acidic residues in the turn between transmembrane segments 1 and 2 (in particular D143) and a basic residue located at the outer end of transmembrane helix 3 (R315). R315 is the only positively charged residue at the extracytoplasmic end of transmembrane segments 3 and 4 which is absolutely conserved among the fungal ATPases (Wach *et al.*, 1992). This places transmembrane segment 3 in the groove between transmembrane segments 1 and 2 on the opposite face of transmembrane segment 8 (Fig. 6). A further consequence of this disposition is that N154 in transmembrane segment 2 can form a hydrogen bond with T304 in transmembrane segment 3. In addition, like the photo-

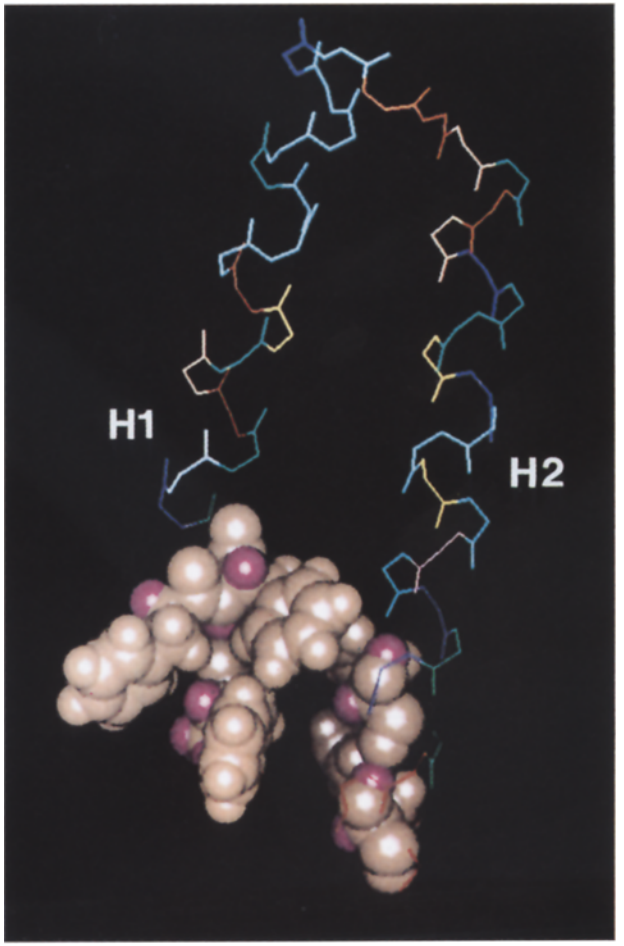

Fig. 5. Distribution and interaction of aromatic side groups at the cytoplasmic end of the helical hairpin. Geometry possible for aromatic side groups (F116, F119, F120, F126, F159, F163) in the aromatic slipper region resulting in favorable π–π interactions.

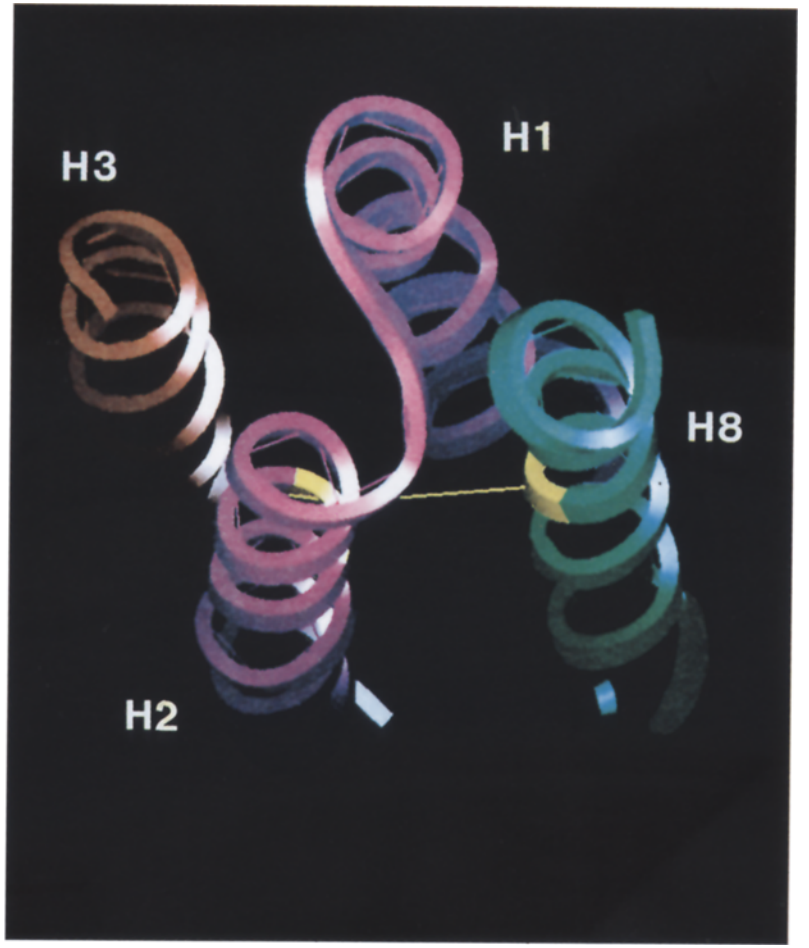

Fig. 6. Juxtaposition of transmembrane segments 1, 2, 3, and 8. Ribbon diagram showing the interaction of transmembrane segments 3 and 8 with the helical hairpin comprising transmembrane segments 1 and 2. The assignment of residues G292-Y314 to helix (red) and residues V858-F882 to helix 8 (green) is based on an eight-helix model, as modified from Nakamoto *et al.* (1989). The view is from the extracytoplasmic face of the membrane perpendicular to the plane of the bilayer. The putative disulfide linkage between C148 and C867 is indicated in yellow.

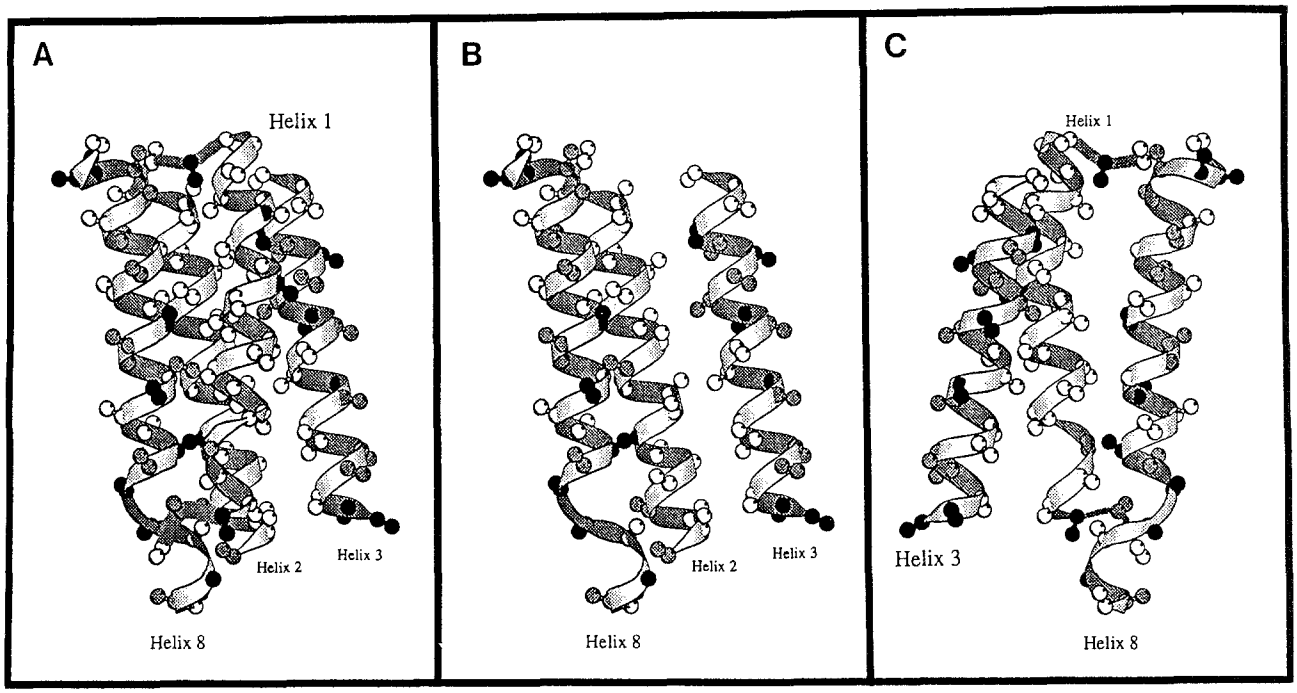

Fig. 7. Analysis of conserved and nonconserved residues in the model containing transmembrane helices 1, 2, 3, and 8. (A) The circles show the location of the α and β carbons for each amino acid over a ribbon trace of the amino acid backbone for each helix, as indicated. All conserved residues are given by the open circles; conservative substitutions are given by the shaded circles, and nonconserved residues are given by the solid circles. Of the nonconserved residues, the residues in the shaded circles are conservative substitutions when all members of the set for each residue fall within only one of the following groupings: (M, I, L, V, F), (F, Y, W), (H, R, K), (N, D, E, Q), an (S, T, A, G). (B) transmembrane segment 1 has been removed to expose the interior faces of transmembrane segments 2, 3, and 8 of the modeled backbone. (C) View obtained by rotating transmembrane segments 1, 2, 3, and 8 by 180° and then removing transmembrane segment 2 in order to look inside the modeled structure.

synthetic reaction center, the four transmembrane segment model locates all of its tryptophan residues at or near the surface of the bilayer. Other possible orientations of helix 3 with helices 1, 2, and 8 were considered, but the arrangement in Fig. 6 was most consistent with conserved features of the hairpin model and existing second-site suppressor data suggesting a direct interaction between helices 1, 2, and 4 (Na *et al.*, 1993).

Comparative analysis of the database of fungal *PMA1* sequences has been used to test aspects of the four-helix model of the ATPase membrane sector (Fig. 7). It can be shown that conserved residues are clustered in strips along closely juxtaposed portions of helices while nonconserved residues are found on surfaces that are in less tight contact. When predominantly nonconserved residues within a strip occupy regions of close contact, it is observed that the conservatively substituted residues are involved. One exception is a cysteine in transmembrane segment 3 which can be replaced by either serine or an alanine. In this instance, compensatory coordinated changes occur within transmembrane segment 3 rather than between helices. The minor effects of evolutionary change on interacting molecular structures in the ATPase membrane sector are consistent with the photosynthetic reaction center proteins where juxtaposed faces of membrane helices are highly conserved, while less constrained surfaces show greater variability.

CONCLUSION

A molecular structure model for transmembrane segments 1 and 2 of the fungal H^+-ATPase has been developed and tested by applying computational, genetic, and biochemical analyses. The helical hairpin structure constructed for this region is conformationally sensitive and highly coupled. The simple four amino acid S-shaped turn region is predicted to be the least constrained and most confor-

mationally heterogeneous region of the structure, but it is also closely coupled to helices 1 and 2, because perturbations in the turn region are propagated to the helices. The region around the turn is closely packed and mutations in this region are expected to alter the hydrogen bonding profile of the hairpin structure. The mutation-induced structural displacements within the helical hairpin are expected to be local, as in the case of A135V, or more global as observed with A135F. Our analysis suggests that this tightly packed conformationally sensitive region of the yeast ATPase near the cell surface, like similar sites on the Na^+,K^+-ATPase and gastric H^+,K^+-ATPase, communicates conformational deformations to the active site. Thus, the displacements observed by the A135V and A135F mutations, which are manifested biochemically as a poorly active enzyme, may be relevant to the binding of function-inactivating drugs, ouabain and SCH28080, to this region in the related Na^+,K^+-ATPase and H^+,K^+-ATPase.

The model analysis has also been valuable in identifying an array of interdigitating aromatic residues that may contribute to the folding of the membrane sector and may provide a mechanistic basis for the effect of membrane potential on the activity of the fungal H^+-ATPase. Finally, in the absence of physical structural data, computationally-derived molecular structure models provide a framework in which to design genetic experiments aimed at exploring the structure and function of the ATPase membrane sector that will ultimately complement experimental efforts directed at solving P-type ATPase structure.

ACKNOWLEDGMENTS

We would like to acknowledge support from NIH Grant GM 38225 to DSP, NIH Grant GM 39737 to JEH, and a grant of the Health Research Council of New Zealand to BCM. CJM received support from a Wellcome-HRC of New Zealand Fellowship. We would like to thank Dr. Harel Weinstein for his support and the generous use of his molecular modeling facility. Finally, we are grateful to Amy Perlin and the Xerox Corporation for generously providing color photocopies of the figures.

REFERENCES

Arystarkhova, E., Gasparian, M., Modyanov, N. N., and Sweadner, K. J. (1992). *J. Biol. Chem.* **19**, 13694–13701

Bigelow, D. J., and Inesi, G. (1991). *Biochemistry* **30**, 2113–2125.

Brandl, C. J., and Deber, C. M. (1986). *Proc. Natl. Acad. Sci. USA* **83**, 917–921.

Canessa, C. M., Horisberger, J.-D., and Rossier, B. C. (1992). *EMBO J.* **11**, 1681–1687.

Chou, K.-C., Maggiora, G. M., Nemethy, G., and Schegara, H. A. (1988). *Proc. Natl. Acad. Sci. USA* **85**, 4295–4299.

DeGrado, W. F., Wasserman, Z. R., and Lear, J. D. (1989). *Science* **243**, 622-628.

Eriksson, A. E., Baase, W. A., Zhang, X.-J., Heinz, D. W., Blaber, M., Blaldwin, E. P., and Mathews, B. W. (1992). *Science* **255**, 178–183.

Feschenko, M. S., Zvaritch, E. I., Hofmann, F., Shakhparonov, M. I., Modyanov, N. N., Vorherr, T., and Carafoli, E. (1992). *J. Biol. Chem.* **267**, 4097–4101.

Findlay, J. B. C., Eliopoulos, E. E., and Finbow, M. (1990). *Biochem. Soc. Trans.* **18**, 838–840.

Forbush, B., III (1983). *Curr. Top. Membr. Transp.* **19**, 167–201.

Glynn, I. M., and Karlish, S. J. D. (1990). *Annu. Rev. Biochem.* **59**, 171–205.

Harris, S. L., Perlin, D. S., Seto-Young, D. and Haber, J. E. (1991). *J. Biol. Chem.* **266**, 24439–24445.

Hennesey, J. P., and Scarborough, G. A. (1990). *J. Biol. Chem.* **265**, 532–537.

Hunter, C. A., and Sanders, J. K. M. (1990). *J. Am. Chem. Soc.* **112**, 5525–5534.

Hunter, C. A., Singh, J., and Thornton, J. M. (1991). *J. Mol. Biol.* **216**, 1–10.

Kanei-Ishii, C., Sarai, A., Sawazaki, T., Nakaghoshi, H., He, D.-N., Ogata, K., Nishimura, Y., and Ishii, S. (1990). *J. Biol. Chem.* **265**, 19990–19995.

Karplus, M., and Petsko, G. A. (1990). *Nature (London)* **347**, 631–639.

Kirley, T. L., and Peng, M. (1991). *J. Biol. Chem.* **266**, 19953–19957.

MacLennan, D. H., Brandl, C. J., Korczak, B., and Green, N. M. (1985). *Nature (London)* **316**, 696–700.

Mandala, S. M., and Slayman, C. W. (1989). *J. Biol. Chem.* **264**, 16276–16282.

Mata, A. M., Matthews, I., Tunwell, R. E. A., Sharma, R. P., Lee, A. G., and East, J. M. (1992). *Biochem. J.* **286**, 567–580.

Miller, M. J., Oldenburg, M., and Fillingame, R. H. (1990). *Proc. Natl. Acad. Sci. USA* **87**, 4900–4904.

Modyanov, N., Lutsenko, S., Chertova, E., Efremov, R., and Gulyaev, D. (1992). *Acta Physiol. Scand.* **146**, 49–58.

Monk, B. C., Montesinos, C., Ferguson, C., Leonard, K., and Serrano, R. (1991). *J. Biol. Chem.* **266**, 18097–18103.

Munson, K. B., Gutierrez, C., Balaji, V. N., Ramnarayan, K., and Sachs, G. (1991). *J. Biol. Chem.* **266**, 18976–18988.

Na, S., Perlin, D. S., Seto-Young, D., Wang, G., and Haber, J. B. (1993). *J. Biol. Chem.* **268**, 11792–11797.

Nakamoto, R., Rao, R., and Slayman, C. W. (1989). *Anal. N.Y. Acad. Sci.* **574**, 165–179.

Perlin, D. S., Brown, C. L., and Haber, J. E. (1988). *J. Biol. Chem.* **263**, 18118–18122.

Price, E. M., Rice, D. A., and Lingrel, J. B. (1989). *J. Biol. Chem.* **264**, 21902–21906.

Price, E. M., Rice, D. A. and Lingrel, J. B. (1990). *J. Biol. Chem.* **265**, 6638–41.

Rabon, E. C., Bin-Im, W., and Sachs, G. (1988). *Methods-Enzymol.* **157**, 649–54.

Rao, U. S., and Scarborough, G. A. (1990). *J. Biol. Chem.* **265**, 7227–7235.

Rao, U. S., Hennessey, J. P., and Scarborough, G. A. (1991). *J. Biol. Chem.* **266**, 14740–14746.

Richardson, J. S., and Richardson, D. C. (1988). *Science* **240**, 1648–1652.

Sachs, G., Besancon, M., Shin, J. M., Mercier, F., Munson, K., and Hersey, S. (1992). *J. Bioenerg. Biomembr.* **24**, 301–308.

Sali, A., Overington, J. P., Johnson, M. S., and Blundell, T. L. (1990). *Trends Biochem. Sci.* **15**, 235–240.

Serrano, R. (1988). *Biochim. Biophys. Acta* **947**, 1–28.

Serrano, R., and Portillo, F. (1990). *Biochem. Biophys. Acta* **1081**, 195–199.

Serrano, R., Kielland-Brandt, M. C., and Fink, G. R. (1986). *Nature (London)* **319**, 689–693.

Seto-Young, D., and Perlin, D. S. (1991). *J. Biol. Chem.* **266**, 1383–1389.

Seto-Young, D., Monk, B. C., and Perlin, D. S. (1992). *Biochim. Biophys. Acta* **1102**, 213–219.

Shull, G. E. and Lingrel, J. B. (1986). *J. Biol. Chem.* **261**, 16788–16791.

Suga, H., Shirabe, K., Yamamoto, T., Tasumi, M., Umeda, M., Nishimura, C., Nakazawa, A., Nakanishi, M., and Arata, Y. (1991). *J. Biol. Chem.* **266**, 13537–13543.

Thornton, J. M., and Gardner, S. P. (1990). Protein Motifs and Database Searching. *Protein: Form and Function*, Elsevier Trends Journals, Cambridge, pp. 153–161.

Wach, A., Schlesser, A., and Goffeau, A. (1992). *J. Bioenerg. Biomembr.* **24**, 309–317.